Acknowledgment. I acknowledge helpful discussions with Dr. M. K. Holloway of Merck Sharp and Dohme Research Laboratories.

Registry No. PMMA, 9011-14-7; PVC, 9002-86-2; methyl chloride, 74-87-3; formic acid, 64-18-6; methane, 74-82-8; methyl acetate, 79-20-9; isopropyl chloride, 75-29-6.

Supplementary Material Available: A listing of AM1 and 6-31G** z matrices and interatomic distances for **1–4** and **9–12** (12 pages). Ordering information is given on any current masthead page.

Balanced Geometries and Structural Trends in Covalent, Ionic, and van der Waals Clusters

David J. Wales

Contribution from the University Chemical Laboratories, Lensfeld Road, Cambridge CB2 1EW, United Kingdom. *Received November 13, 1989*

Abstract: Leech's defintion of a balanced structure is refined and extended with use of a simple group theoretical proof. Hence the conditions for a given molecular structure to be in tangential equilibrium under an arbitrary force law are deduced, and the possible orbits are enumerated. The conclusions are verified for a variety of different covalent, ionic, and van der Waals clusters by direct calculation, including stationary points of order 0 to 24. A systematic set of results is also presented for argon clusters including more than 50 stationary points that have been studied with both a Lennard-Jones and a much more accurate potential function involving three-body interactions. The influence of the form of the potential upon the order of the stationary points and upon the geometries of minima and transition states in particular is then discussed.

I. Introduction

Recent investigations of potential energy surfaces[1,2] have revealed some very interesting trends and similarities in the shapes of different kinds of clusters. Furthermore, the relationships between the different systems are not confined to shape alone; similarities in topology of potential energy surfaces also imply relationships in the dynamical processes that the systems exhibit. For example, it was found that most of the low-energy rearrangements exhibited by argon and "trapped ion" clusters can be described in terms of Lipscomb's diamond-square-diamond mechanism[3] (both systems) or Johnson's edge-bridging mechanism[4] (argon clusters only). Such results are of great importance in developing a detailed understanding[5] of the liquid/solid coexistence behavior of small argon clusters,[6] which draws a pleasing parallel with the rationalization of rearrangement rates in *closo*-boranes and carboranes. For the latter systems a topological analysis[7] must be augmented by considerations of orbital symmetry[8] to obtain a complete picture.

Since part of the purpose of this paper is to discuss the similarities and common features of the stationary structures exhibited by different clusters, it will serve us well to introduce some nomenclature. We divide clusters into three classes: (1) covalent clusters (those taken to be such species as boranes, carboranes, and transition-metal clusters); (2) van der Waals clusters (those that include clusters of inert gas atoms such as argon as well as benzene clusters and any other systems in which the binding energy is primarily due to dispersion forces); and (3) ionic clusters (those that include binary alkali halides such as $(KCL)_n$ as well as "trapped ion" clusters; the latter species consist of identical ions held in an attractive well potential[9], which for the present calculations is isotropic and harmonic in form).[1] This scheme may not always be unambiguous, but it will generally be helpful in distinguishing different types of systems in the present work.

In 1957 Leech deduced the conditions for a set of particles confined to the surface of a sphere to be in equilibrium under any pairwise law of force;[10] his geometrical proof enabled all such "balanced" structures to be identified. The necessary and sufficient condition for a structure to be balanced in this sense is that every particle must lie on a rotational axis of the appropriate point group.[10] Balanced structures fall into two classes: (1) all particles equally spaced on a great circle with or without two identical particles at the poles; (2) the particles define the vertices, centers of faces, or mid-points of edges of a regular polyhedron, or any of the three sets taken together. In this report the concept of a balanced structure is extended to systems with arbitrary force laws (which need not be pairwise additive) and to the tangential equilibrium (i.e. the shape) of molecules where the atoms describe more than one orbit of the point group. An orbit of a point group is a complete set of equivalent points that is mapped onto itself (aside from permutations) under all the point group operations. The conclusions are investigated by a series of calculations on a wide variety of different clusters, including a comprehensive survey of stationary points for argon clusters containing 4 to 55 atoms with use of two different potential functions. These results are of interest in dynamical studies of argon clusters where the simpler Lennard-Jones potential is usually employed. The trends that emerge for the two potential functions are discussed in terms of the two-body and three-body contributions; the use of the Lennard-Jones potential should be generally justifiable for dynamical studies as it does not misrepresent the important features of the potential energy surface in any of the cases studied. Finally, the

(1) Wales, D. J. *J. Chem. Phys.* **1989**, *91*, 7002.
(2) Wales, D. J. *Chem. Phys. Lett.* **1990**, *166*, 419.
(3) Lipscomb, W. N. *Science (Washington D.C.)* **1966**, *153*, 373.
(4) Johnson, B. F. G. *J. Chem. Soc., Chem. Commun.* **1986**, 27.
(5) Berry, R. S.; Wales, D. J. *Phys. Rev. Lett.* **1989**, *63*, 1156. Wales, D. J.; Berry, R. S. *J. Chem. Phys.* **1990**, *92*, 4473.
(6) Hahn, M. Y.; Whetten, R. *Phys. Rev. Lett.* **1988**, *61*, 1190. Berry, R. S.; Jellinek, J.; Natanson, G. *J. Phys. Rev. A* **1984**, *30*, 919. Beck, T. L.; Berry, R. S. *J. Chem. Phys.* **1986**, *84*, 2783. Davis, H. L.; Jellinek, J.; Berry, R. S. *J. Chem. Phys.* **1987**, *86*, 6456. Beck, T. L.; Jellinek, J.; Berry, R. S. *J. Chem. Phys.* **1987**, *87*, 545. Reiss, H.; Mirabel, P.; Whetton, R. L. *J. Phys. Chem.* **1988**, *92*, 7241. Bixon, M.; Jortner, J. *J. Chem. Phys.* **1989**, *91*, 1631.
(7) King, R. B. *Inorg. Chim. Acta* **1981**, *49*, 237.
(8) Wales, D. J.; Stone, A. J. *Inorg. Chem.* **1987**, *26*, 3845.
(9) Schiffer, J. P. *Phys. Rev. Lett.* **1988**, *61*, 1843. Levi, B. G. *Phys. Today* **1988**, *41*, 17. Rahman, A.; Schiffer, J. P. *Phys. Rev. Lett.* **1986**, *57*, 1133.
(10) Leech, J. *Math. Gazette* **1957**, *41*, 81.

0002-7863/90/1512-7908$02.50/0

relation of structural trends in different clusters to the qualitative form of the potential functions is discussed. The origins of structural isomorphisms and of diversity in clusters can generally be related to familiar chemical concepts, although the change in the order of stationary points with the same geometry is less well understood. The latter will be the subject of a separate report.[11] Knowledge that a stationary point of some order is bound to exist for a particular geometry may serve to guide future ab initio studies as well as structural investigations of conceptually simpler ionic and van der Waals clusters.

II. Balanced Structures

We first review Leech's most important result, namely that systems of points confined to a spherical surface are in equilibrium under any pairwise force law if there is a rotation axis through each one. First notice that we will not be concerned with radial forces. The latter do not affect the *shape* of the system but instead determine whether or not there can be a bound stationary point at all. It is reasonable to assume that practically all systems of chemical interest do indeed have such a bound state, as we shall see.

Before extending the basic result let us consider a simple geometrical proof that subsumes Leech's approach. We will show that angular equilibrium exists for any pairwise resolvable force if every point lies on a rotational axis. The centers for the forces do not in fact have to be on the other atoms, so long as the former are an orbit of the point group. Consider any point, i, which lies on a rotation axis of order n. The remaining points must be arranged in rings of n or $2n$ equivalent sites in planes that are perpendicular to the rotation axis through i. ($2n$ equivalent points can arise, for example, in the D_{nd} and D_{nh} point groups when the atoms do not lie on the perpendicular rotation axes.) Any other points that lie on the same rotational axis clearly contribute no tangential force at point i. The force on atom i due to any of the n or $2n$ equivalent sites in a ring can be decomposed into two orthogonal tangential components, and the net force along both these arbitrary directions vanishes because

$$\sum_{m=0}^{n-1} \begin{Bmatrix} \cos(2m\pi/n) \\ \sin(2m\pi/n) \end{Bmatrix} = 0$$

which follows from summing the geometric progression

$$\sum_{m=0}^{n-1} e^{2m\pi i/n}$$

and taking the real and imaginary parts.

Since no assumptions were made about the radii of the sets of equivalent points we can immediately generalize this result to structures containing more than one orbit of the required type, where again the particles interact by pairwise decomposable forces. Here we assume that suitable radial distances for the different orbits exist so that the stationary point is bound. This is clearly the case for ligated clusters such as cubane, C_8H_8, and icosahedral $B_{12}H_{12}^{2-}$. Here we may also include structures consisting of a regularly spaced ring of atoms with two equivalent polar atoms, such as pentagonal bipyramidal Ar_7. However, the polar atoms do not have to lie on the same sphere as the atoms in the equatorial ring and do not even have to be the same kind of atoms at all. Many more detailed examples will be given in the next section. First, however, we use group theory to show that the results are actually applicable to systems with arbitrary force laws, not just to pairwise additive potentials. Hence we may treat covalent clusters on the same footing as systems governed by purely ionic forces, for example. This was implicitly assumed in the examples given for two-orbit systems above.

A symmetry analysis is needed to encompass general force laws, including systems that must be treated quantum mechanically, such as borohydrides and most transition-metal clusters. The components of the gradient of the energy, $\partial E/\partial Q_i$, where Q_i is a Cartesian displacement coordinate of any atom, clearly form a basis for a representation of the molecular point group. In fact, the subset of components including only displacements of atoms in any orbit also forms such a basis, because only these components are transformed into one another under operations of the point group. For a nondegenerate electronic state the expectation value of this gradient vector vanishes unless it contains a part that transforms as the totally symmetric irreducible representation of the point group, Γ_0. If the vector vanishes then so do its components, so that if there are to be nonvanishing forces on sets of equivalent atoms then the basis set $\{\partial E/\partial Q_i\}$ must contain Γ_0. If we divide the local displacements Q_i into radial and tangential components then it is clear[12] that the representation spanned by the former always includes Γ_0. However, if the representation spanned by the tangential components does not contain Γ_0 then the orbit is in tangential equilibrium for an arbitrary force law and is therefore balanced.

Fowler and Quinn have tabulated the transformation properties of a set of tangential unit vectors for the orbits of all the chemically important point groups.[12] Only the orbits that do not contain Γ_0 in the tangential unit vector representation can form part of a balanced structure. These orbits are the same as those deduced by Leech's geometrical construction and are summarized in Table I.

Table I. Point Groups and Their Tangentially Balanced Orbits, O_n[a]

point group	orbits	point group	orbits
I_h	O_{12}, O_{20}, O_{30}	D_{5h}	O_2, O_5
$C_{\infty v}$	O_1	D_{4h}	O_2, O_4
$D_{\infty h}$	O_2	D_{3h}	O_2, O_3
I	O_{12}, O_{20}, O_{30}	D_{2h}	$O_{2x,2y,2z}$
O_h	O_6, O_8, O_{12}	C_{6h}	O_2
O	O_6, O_8, O_{12}	C_{5h}	O_2
T_h	O_6, O_8	C_{4h}	O_2
T_d	O_4, O_6	C_{3h}	O_2
T	O_4, O_6	C_{2h}	O_2
S_6	O_2	$C_{2v,3v,4v,5v,6v,\ldots}$	O_1
S_4	O_2	D_6	O_2, O_6
D_{6d}	O_2, O_{12}	D_5	O_2, O_5
D_{5d}	O_2, O_{10}	D_4	O_2, O_4
D_{4d}	O_2, O_8	D_3	O_2, O_3
D_{3d}	O_2, O_6	D_2	$O_{2x,2y,2z}$
D_{2d}	O_2, O_4	$C_{2,3,4,5,6,\ldots}$	O_1

[a] n is the number of equivalent sites in the oribt. These are simply the orbits for which the tangential unit vector representation[12] does not contain the totally symmetric irreducible representation of the point group. O_1 is omitted for brevity except for the groups where it is the only balanced orbit.

In the following sections we will address several questions that immediately come to mind. First, in section III, a series of example calculations are presented that include stationary points of order zero (minima), order one (true transition states[13]), and a number of higher order saddles. Throughout this paper we associate the order of a stationary point or saddle point with the number of negative eigenvalues of the Hessian or second derivative matrix at that geometry. Then, in section IV, a systematic survey of stationary points of various orders is presented for a range of more than 50 different argon cluster geometries with 4 to 55 atoms. In section V we examine the important question of how the qualitative nature of the potential governs the order of the balanced stationary points and how it affects the types of unbalanced structures that are minima for different types of clusters. These questions are clearly of fundamental importance in understanding structural trends and reaction dynamics in all branches of cluster chemistry, and the present theoretical framework provides a unified viewpoint in which to frame such studies. We also note that this framework may be extended to higher derivatives of the energy to identify the maximum number of independent non-zero components. The detailed proofs will be presented elsewhere, along with some applications to ab initio chemistry.

(11) Braier, P. A.; Wales, D. J.; Berry, R. S. *J. Chem. Phys.* In press.

(12) Fowler, P. W.; Quinn, C. M. *Theor. Chim. Acta* **1986**, *70*, 333.

(13) Murrell, J. N.; Laidler, K. J. *Trans. Faraday Soc.* **1968**, *64*, 371.

Table II. Examples of Balanced Structures for Covalent, Ionic, and van der Waals Clusters[a]

point group; orbit	structure	examples
D_{3h}; O_3	equilateral triangle	Ar_3 [0][a], $(Be^+)_3^1$ [0][b], $(CH)_3^+$ [0]
$D_{\infty h}$; O_2, O_1	linear	HC≡CC≡CH [0]
T_d; O_4	tetrahedron	Ar_4 [0][a], $(Be^+)_4^1$ [0][a], $(BCl)_4$ [0], P_4 [0]
D_{4h}; O_4	square	Ar_4 [2][a], $(Be^+)_4^1$ [1][a]
D_{3h}; O_3, O_2	trigonal bipyramid	Ar_5 [0][a], $Be^+)_5^1$ [0][a], $C_5H_5^+$ [5][b], $C_5H_5^-$ [5][b]
D_{5h}; O_5	pentagon	Ar_5 [4][a], $(Be^+)_5^1$ [2][a], $C_5H_5^-$ [0]
O_h; O_6	octahedron	Ar_6 [0][a], $(Be^+)_6^1$ [0][a], $B_6H_6^{2-}$ [0]
D_{6h}; O_6	hexagon	Ar_6 [6][a], $(Be^+)_6^1$ [4][a], C_6H_6 [0]
D_{5h}; O_5	pentagonal bipyramid	Ar_7 [0][a], $(Be^+)_7^1$ [0][a], $B_7H_7^{2-}$ [0]
D_{7h}; O_7	heptagon	Ar_7 [8][a], $(Be^+)_7^1$ [6][a]
O_h; O_8	cube	Ar_8 [6][a], $(Be^+)_8^1$ [2][a], C_8H_8 [0]
D_{6h}; O_6, O_2	bicapped hexagon	Ar_8 [3][a], $(Be^+)_8^1$ [3][a]
I_h; O_{12}	icosahedron	$B_{12}H_{12}^{2-}$ [0]
O_h; O_{12}	cuboctahedron	Ar_{12} [6][a], $(Be^+)_{12}^1$ [1][a], $B_{12}H_{12}^{2-}$ [4][b]
I_h; O_{12}, O_1	centered icosahedron	Ar_{13} [0][a], $(Be^+)_{13}^1$ [0][a]
I_h; O_{20}	dodecahedron	$C_{20}H_{20}$ [0]
I_h; O_{30}	icosidodecahedron	Ar_{30} [24][a]
I_h; O_{20}, O_{12}, O_1	centered, stellated icosahedron	Ar_{30} [0][a]

[a] The order of each stationary point is given in brackets after the formula, and the orbits of the point group present are noted in the first column. Superscript a denotes calculations performed with the Cerjan-Miller method[1] (some of the results are also known from earlier work[14]); superscript b denotes ab initio calculations performed with CADPAC[22] using STO-3G basis sets; the other structures are well-known minima. $(Be^+)_n^1$ clusters are systems containing n Be^+ ions contained by a central harmonic potential.

III. Some Examples of Balanced Structures

The calculations that led to some of the trends reported herein first coming to the author's attention have been reported elsewhere.[1] The objective of the latter study was primarily to calculate transition-state geometries and thereby relate dynamical processes (as simulated by the method of molecular dynamics) to details of the potential energy surfaces. Finding minima on potential surfaces is a much easier task; for example, a wide variety of minima have been well-known for argon clusters for some time.[14] Some of the transition states for Ar_7 were recently calculated by using the "Slowest Slides" technique adapted from the methodology of molecular dynamics.[15] However, a much wider set of results has since been obtained on applying the Cerjan–Miller eigenvector-following method[16] to ionic and van der Waals clusters.[1] These calculations will be used in forth-coming reports of dynamical processes for potassium chloride,[17] "trapped ion",[18] bare metal clusters,[11] and argon clusters,[19] as well as in a study of the Carter–Handy potential surface[20] for formaldehyde in which we compare the behavior of the Cerjan–Miller and Slowest Slide approaches.[21]

The results reported in this section were obtained by using the Cerjan–Miller method in the case of ionic and van der Waals clusters and with the CADPAC ab initio package[22] for the covalent clusters. For the latter systems all the calculations were symmetry constrained so that they could be run as minimizations. CADPAC performs well under these conditions, whereas it does not seem to locate transition states for clusters of similar sizes in unconstrained searches very readily.[23] It is interesting to note that we are sure to find a stationary point of some variety in each case, although the order of the stationary point may vary depending upon the basis set and the charge on the cluster. All the results in Table II were found with use of minimal STO-3G bases.

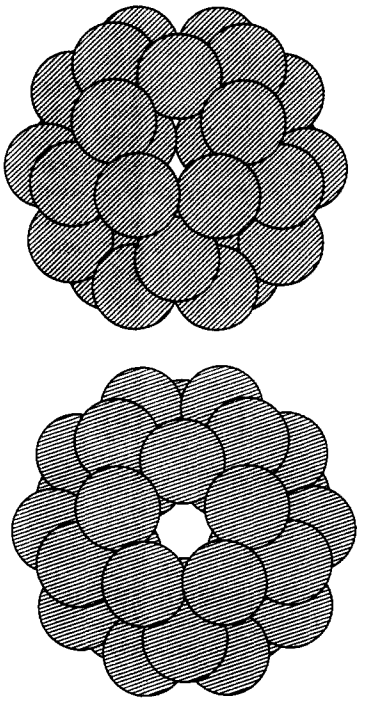

Figure 1. Two views of the Ar_{30} icosidodecahedron; O_{30} in I_h is the largest balanced orbit of any point group normally encountered.

For the ionic and van der Waals clusters minima and transition states were generally located with unconstrained searches as described elsewhere.[1] However, the package adapted for these calculations[24] also allows for symmetry contraints that were employed to find the higher order saddles. Results for a variety of systems, some familiar and some hypothetical, are given in Table II. Examples are provided for all the orbits of the cubic groups, and since the icosidodecahedron will probably not be known to most readers it is illustrated in Figure 1. The trends that emerge in this section and in section IV are discussed in section V. The results show that we can indeed find stationary points of some order for molecules with balanced geometries, whatever the nature of the bonding. Only if the potential is repulsive (or the electronic

(14) Hoare, M. R.; Pal, P. *J. Cryst. Growth* **1972**, *17*, 77.
(15) Berry, R. S.; Davis H. L.; Beck, T. L. *Chem. Phys. Lett.* **1988**, *147*, 13.
(16) Cerjan, C. J.; Miller, W. H. *J. Chem. Phys.* **1981**, *75*, 2800. Simmons, J.; Jørgenson, P.; Taylor, H.; Ozment, J. *J. Phys. Chem.* **1983**, *87*, 2745. O'Neal, D.; Taylor, H.; Simmons, J. *J. Phys. Chem.* **1984**, *88*, 1510. Baker, J. *J. Comp. Chem.* **1986**, *7*, 385. Baker, J. *J. Comp. Chem.* **1987**, *8*, 563.
(17) Rose, J.; Berry, R. S.; Wales, D. J. To be published.
(18) Rafac, R.; Schiffer, J. P.; Wales, D. J. In preparation. Rafac, R.; Schiffer, J. P.; Hargst, J.; Dubis, D.; Wales, D. J. *Proc. Natl. Acad. Sci. U.S.A.* Submitted.
(19) Wales, D. J.; Berry, R. S. *J. Chem. Phys.* **1990**, *92*, 4283.
(20) Handy, N. C.; Carter, S. *Chem. Phys. Lett.* **1981**, *79*, 118.
(21) Davis, H. L.; Wales, D. J.; Berry, R. S. *J. Chem. Phys.* **1990**, *92*, 4308.
(22) Amos, R. D.; Rice, J. E., CADPAC: *Cambridge Analytic Derivatives Package*, Issue 4; Cambridge University: Cambridge, England, 1987.
(23) Wales, D. J. Unpublished studies.
(24) ACES (Advanced Concepts in Electronic Structure)—An Ab Initio Program System, authored by Bartlett, R. J.; Purvis, G. D.; Fitzgerald, G. B.; Harrison, R. J.; Lee, Y. S.; Laidig, W. D.; Cole, S. J.; Trucks, G. W.; Magers, D. H.; Salter, E. A.; Sosa, C.; Rittby, M.; Pal, S.; Stanton, J. F.

wavefunction is degenerate) for any size of the cluster with the given shape will there not be a stationary point for finite cluster size.

IV. Systematic Study of Stationary Points for Two Argon Potentials

The minima and transition states reported previously[1] were all computed with a Lennard-Jones potential[25]

$$V = 4\epsilon\sum_{i<j}\left(\left(\frac{\sigma}{r_{ij}}\right)^{12} - \left(\frac{\sigma}{r_{ij}}\right)^{6}\right)$$

where r_{ij} is the distance between atoms i and j, ϵ is the well depth, and σ is the pair separation for which $V(r_{ij})$ vanishes. While this potential is widely used it is known that the actual interactions between argon atoms are significantly different from those described by the above form.[26] However, potentials including three- as well as two-body interactions are available for which calculated properties of solid, liquid, and gaseous argon are in very good agreement with experiment.[27] The more accurate potential employed for this study utilized the two-body form of Barker and Pompe[28]

$$V_2 = \epsilon\sum_{i<j}\left[e^{12.5(1-\rho_{ij})}\{0.2349 - 4.7735(\rho_{ij}-1) - 10.2194(\rho_{ij}-1)^2 - 5.2905(\rho_{ij}-1)^3\} - \frac{1.0698}{0.01+\rho_{ij}^{6}} - \frac{0.1642}{0.01+\rho_{ij}^{10}} - \frac{0.0132}{0.01+\rho_{ij}^{12}}\right]$$

where the well depth $\epsilon = 2.040 \times 10^{-14}$ erg (1 erg = 1×10^{-7} J) and ρ_{ij} is the separation of atoms i and j divided by the separation at the equilibrium distance for the argon dimer described by this function, which is 3.7560 Å. For the three-body term the Axilrod–Teller triple-dipole form was used[29]

$$V_3 = \nu\sum_{i<j<k}\frac{1 + 3\cos\theta_1\cos\theta_2\cos\theta_3}{(R_1R_2R_3)^3},$$

where $\nu = 73.2 \times 10^{-12}$ erg Å^9 and the R_i and θ_i are the side lengths and internal angles of the triangle ijk, respectively.[27] This interaction is generally destabilizing for triangles with only acute angles and stabilizing otherwise. Quantum corrections of the type applied by Barker, Fisher, and Watts[27] were not included as they are not expected to change the results significantly.

The overall form chosen for the potential was governed by two considerations: first, a desire to compare the Lennard-Jones results with a more accurate potential including three-body corrections, and second, computational practicality. For clusters of the size of Ar_{55} optimizations become rather expensive, so that a compromise must be found between accuracy and complexity. The neglect of three-body terms other than the triple-dipole is a sensible step, as demonstrated by Etters and Danilowicz's previous calculations.[30] The latter work serves as a helpful check on the present calculations which include a much wider range of structures and, of course, stationary points of higher order. Optimizations for clusters as large as Ar_{55} were feasible with use of analytic gradients and Hessians for the Lennard-Jones potential and analytic gradients combined with two-sided numerical differentiation for the Hessian in the case of the more complicated potential. Only the calculations of saddles of order two or more involved any constraints, and all the results were checked by examining the eigenvalues of the full Cartesian Hessian. The magnitudes of the six "zero" eigenvalues and the number of negative eigenvalues enable the convergence of the calculation and the order of the stationary point to be monitored.[1]

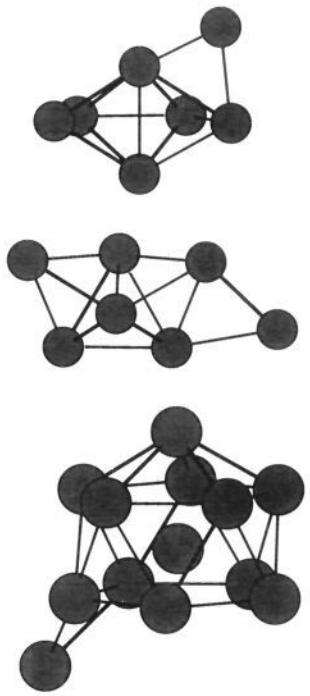

Figure 2. Structures that are transition states for the Lennard-Jones potential but not for the more accurate many-body potential described in the text. Note that in every case an edge-bridging atom is present.

The results are tabulated in Table III for a Lennard-Jones potential with the same well depth, $\epsilon = 2.040 \times 10^{-14}$ erg, as for the Barker–Pompe two-body interaction. The Lennard-Jones energies can, of course, be rescaled for an arbitrary well depth ϵ' by multiplying by ϵ'/ϵ. The present choice is appropriate for comparison with the chosen many-body form in order to highlight the effects of the three-body interactions. These are two distinct points for discussion in these results: (1) comparison of the stationary points and their orders with the two different potentials; and (2) analysis of the detailed energetic changes of the equivalent stationary points (where they exist). It is important to realize that the values of the particular Lennard-Jones ϵ and σ parameters are irrelevant to the discussion of point 1, that is, they play no part in determining the *topology* of the Lennard-Jones potential surfaces. On the other hand, in analyzing the detailed energetic differences between equivalent stationary points it is appropriate to consider a Lennard-Jones poential with the same well depth as the two-body Barker–Pompe form so that the effects of the three-body terms are not obscured. The choice of the Lennard-Jones σ was only significant in that the optimizations with the many-body potential were started from the corresponding Lennard-Jones geometries. Using a pair equilibrium separation some 1.6% larger than that of the Barker–Pompe form allowed for some structural relaxation and generally resulted in efficient convergence to the equivalent stationary points with the more complex potential.

Consider first the changes in topology of the potential energy surfaces, for which the Lennard-Jones scaling parameters play no part. All of the reoptimized stationary points have the same order with the two different potentials, except that in three cases the stationary point disappears completely. The latter geometries are all of the edge-bridging type[4] and are illustrated in Figure 2. To check whether the two-body or the three-body part of the potential is responsible for these results reoptimization was attempted with the two-body term only. Again no stationary point was found in each case. Since all the reoptimizations were started from the converged Lennard-Jones geometries corresponding to a very similar equilibrium pair separation, this strongly indicates that these particular stationary points simply are not present for

(25) Lennard-Jones, J. E. *Proc. R. Soc. A* **1924**, *106*, 463.
(26) Guggenheim, E. A.; McGlashan, M. L. *Proc. R. Soc. A* **1960**, *255*, 456. McGlashan, M. L. *Discuss. Faraday Soc.* **1965**, *40*, 59.
(27) Barker, J. A.; Fisher, R. A.; Watts, R. O. *Mol. Phys.* **1971**, *21*, 657.
(28) Barker, J. A.; Pompe, A. *Aust. J. Chem.* **1968**, *21*, 1683.
(29) Axilrod, B. M.; Teller, E. *J. Chem. Phys.* **1943**, *11*, 299. Axilrod, B. M. *J. Chem. Phys.* **1949**, *17*, 1349. Axilrod, B. M. *J. Chem. Phys.* **1951**, *19*, 719.
(30) Etters, R. D.; Danilowicz, R. *J. Chem. Phys.* **1979**, *71*, 4767.

Table III. Energies (10^{13} erg) for Various Calculated Stationary Points of Argon Clusters Using a Common Pair Potential Well Depth of 2.040 × 10^{-14} erg[a]

structure	E_{LJ}	E_{MB}	ΔE	V_2	V_3	order
Ar_4 square	−0.9139	−0.8779	−0.036	−0.8853	0.007357	2
Ar_5 trigonal bipyramid	−1.857	−1.801	−0.056	−1.848	0.04738	0
Ar_5 square-based pyramid	−1.730	−1.663	−0.067	−1.701	0.03780	1
Ar_5 pentagon	−1.134	−1.085	−0.049	−1.089	0.004158	4
Ar_6 hexagon	−1.334	−1.287	−0.047	−1.288	0.0008364	6
Ar_7 pentagonal bipyramid	−3.367	−3.216	−0.151	−3.322	0.1064	0
Ar_7 capped octahedron	−3.251	−3.091	−0.160	−3.187	0.09620	0
Ar_7 tricapped tetrahedron	−3.182	−3.038	−0.144	−3.131	0.09280	0
Ar_7 bicapped trigonal bipyramid	−3.169	−3.032	−0.137	−3.123	0.091022	0
Ar_7 saddle 1.2.a	−3.118	−2.961	−0.157	−3.049	0.08738	1
Ar_7 saddle 1.2.b	−3.066	−2.910	−0.156	−2.994	0.08370	1
Ar_7 saddle 1.2.c	−3.151	−2.982	−0.169	−3.070	0.08817	1
Ar_7 saddle 1.2.d	−3.125	−2.965	−0.160	−3.053	0.08812	1
Ar_7 saddle 1.2.e	−2.978		stationary point disappears			1
Ar_7 saddle 1.2.f	−2.968		stationary point disappears			1
Ar_7 saddle 21.2.e	−3.067	−2.911	−0.156	−2.995	0.08382	1
Ar_7 saddle 21.2.d	−3.080	−2.921	−0.159	−3.006	0.08531	1
Ar_7 heptagon	−1.535	−1.490	−0.045	−1.488	−0.002051	8
Ar_8 capped pentagonal bipyramid	−4.043	−3.843	−0.200	−3.972	0.1291	0
Ar_8 dodecadeltahedron	−4.032	−3.785	−0.247	−3.899	0.1137	0
Ar_8 C_{2v}-bicapped octahedron	−3.915	−3.712	−0.203	−3.829	0.1167	0
Ar_8 stellated tetrahedron	−3.871	−3.672	−0.199	−3.789	0.1173	0
Ar_8 cube	−3.117	−2.854	−0.263	−2.912	0.05858	6
Ar_8 bicapped hexagon	−3.615	−3.414	−0.201	−3.513	0.09822	3
Ar_8 saddle 1.4.A	−3.934	−3.707	−0.227	−3.828	0.1210	1
Ar_8 saddle 1.4.B	−3.748	−3.543	−0.205	−3.650	0.1066	1
Ar_8 saddle 1.4.C	−3.862	−3.623	−0.239	−3.734	0.1105	1
Ar_8 saddle 1.4.D	−3.758	−3.555	−0.203	−3.659	0.1043	1
Ar_8 saddle 1.4.E	−3.816	−3.600	−0.216	−3.712	0.1126	1
Ar_8 saddle 1.4.F	−3.908	−3.697	−0.211	−3.818	0.1214	1
Ar_{12} cuboctahedron	−5.906	−5.422	−0.484	−5.555	0.1326	6
Ar_{13} icosahedron	−9.043	−8.376	−0.667	−8.758	0.3822	0
Ar_{13} 1.6.B	−8.454	−7.854	−0.600	−8.810	0.3261	0
Ar_{13} 1.6.C	−8.445	−7.850	−0.595	−8.173	0.3233	0
Ar_{13} 1.6.D	−8.460	−7.858	−0.602	−8.181	0.3260	0
Ar_{13} 1.6.E	−8.067	−7.530	−0.537	−7.819	0.2891	0
Ar_{13} 1.6.F	−8.076	−7.496	−0.580	−7.496	0.2891	0
Ar_{13} saddle 1.9.A	−8.345	−7.707	−0.638	−8.022	0.3148	1
Ar_{13} saddle 1.9.B	−8.254	−7.619	−0.635	−7.925	0.3063	1
Ar_{13} saddle 1.9.C	−8.246		stationary point disappears			1
Ar_{13} saddle 1.9.D	−8.048	−7.482	−0.566	−7.768	0.2862	1
Ar_{13} saddle 1.9.E	−8.288	−7.657	−0.631	−7.969	0.3117	1
Ar_{13} saddle 1.9.F	−8.023	−7.437	−0.586	−7.715	0.2776	1
Ar_{14} capped icosahedron	−9.761	−9.026	−0.735	−9.431	0.4051	0
Ar_{14} saddle 1.9.G	−9.374	−8.621	−0.753	−8.984	0.3623	1
Ar_{14} saddle 1.9.H	−9.601	−8.869	−0.732	−9.265	0.3961	1
Ar_{14} saddle 1.9.I	−9.352	−8.602	−0.750	−8.962	0.3603	1
Ar_{14} saddle 1.9.J	−8.760	−8.097	−0.663	−8.401	0.3035	1
Ar_{30} icosidodecahedron	−14.50	−13.38	−1.12	−13.56	0.1820	24
Ar_{33} centered stellated icosahedron	−29.06	−25.59	−3.47	−27.24	1.325	0
Ar_{33} 1.10	−28.60	−25.59	−3.01	−26.79	1.204	0
Ar_{33} saddle 1.10	−28.14	−25.13	−3.01	−26.31	1.173	1
Ar_{55} Mackay icosahedron[32]	−56.90	−50.22	−6.68	−52.96	2.748	0
Ar_{55} minimum 1.11	−55.52	−49.03	−6.49	−51.58	2.551	0
Ar_{55} minimum 2.2	−56.43	−49.71	−6.72	−52.42	2.703	0
Ar_{55} minimum 2.3	−55.79	−49.22	−6.57	−51.86	2.640	0
Ar_{55} minimum 2.4	−56.38	−49.69	−6.69	−52.39	2.698	0
Ar_{55} minimum 2.5	−55.84	−49.25	−6.59	−51.90	2.647	0
Ar_{55} saddle 1.11	−54.10	−47.62	−6.48	−50.09	2.469	1
Ar_{55} saddle 2.2	−55.08	−48.50	−6.58	−51.06	2.559	1
Ar_{55} saddle 2.3	−55.70	−49.10	−6.60	−51.74	2.637	1
Ar_{55} saddle 2.4	−56.15	−49.48	−6.67	−52.16	2.682	1
Ar_{55} saddle 2.5	−55.71	−49.08	−6.63	−51.71	2.633	1

[a] E_{LJ} and E_{MB} are the results for the Lennard-Jones and the more complicated many-body potential described in the text. V_2 and V_3 are the two-body and three-body contributions to the total energy for the latter potential, and $\Delta E = E_{LJ} - E_{MB}$. The order of the stationary points, which is unchanged unless it disappears completely, is given in the last column. To avoid reproducing all the structures references are given to figures in earlier papers for all the unnamed geometries. For example, 21.2.h means ref 21, Figure 2, structure h.

the more accurate potential. In each case there were no negative Hessian eigenvalues in the internal coordinate representation, and optimizations searching for both minima and transition states were therefore performed. The searches for minima simply resulted in collapse to one of the nearby minima. Hence we reach the important conclusion that *the Lennard-Jones potential overestimates the stability of structures containing vertices of low connectivity*. This may be ascribed to the unrealistically large long-range tail of the Lennard-Jones potential; the Axilrod–Teller form will also destabilize the acute-angled triangles formed by edge-bridges in edge-bridged transition states.

Fortunately, all three of the above edge-bridging transition states are high lying relative to the lowest Lennard-Jones minima, so that they are not important in our interpretations of melting

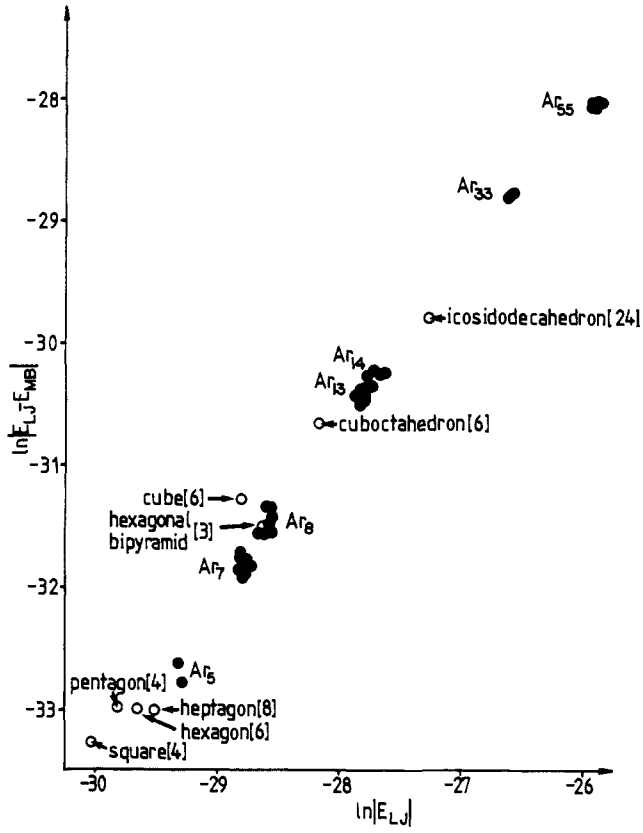

Figure 3. Plot of $\ln |E_{LJ} - E_{MB}|$ against $\ln |E_{LJ}|$ for the calculated energies of Table III. The solid circles are the minima and transition states; the open circles are higher order saddles and are all identified by name with their order in square brackets.

processes.[19] Furthermore, some edge-bridging structures (such as the edge-bridged octahedron and the edge-bridged, centered icosahedron) remains true transition states with the many-body potential. In these cases there is a 2-fold rotation axis through the two-connected atom, so that tangential forces on that atom must vanish by the same arguments as in section II. Hence, although the latter structures are not balanced, it is not surprising that they remain transition states.

Now we consider the detailed energetic trends for the equivalent stationary points where they exist. The change in energy from the many-body to the Lennard-Jones potential (with the same two-body well depth) increases steadily with the Lennard-Jones energy, but not in a linear fashion. However, a plot of $\ln |E_{LJ}|$ against $\ln |E_{LJ} - E_{MB}|$ produces a reasonable fit to a straight line with a correlation coefficient of 0.982 for all 60 data points of Table III (Figure 3). The empirical relationship that may be deduced from this fit is

$$|E^*_{LJ} - E^*_{MB}| \approx e^{\beta}\epsilon^{\alpha-1}|E^*_{LJ}|^{\alpha} \text{ or } |E_{LJ} - E_{MB}| \approx 338.4|E_{LJ}|^{1.307}$$

where the reduced energies are scaled by the pair potential well depth on the left, with $\beta = 5.8242$ and $\alpha = 1.307$, and the energies are in ergs for the unscaled equation on the right calculated with $\epsilon = 2.040 \times 10^{-14}$ erg as recommended for the Barker–Pompe potential and used in Table III.

All the shifts for the many-body potential are to higher energy, and the three-body contributions at the new stationary points are all positive, except for the case of the very open heptagon. The percentage change in energy may also be analyzed separately for the minima and the transition states, and the averaged results are summarized in Table IV. From these we see that the percentage shifts are usually a little larger for the transition states of a given nuclearity than for the minima. Since the transition-state energies are numerically smaller than the energies of the corresponding minima, this means that conclusions about barriers deduced from the Lennard-Jones potential will generally be qualitatively correct. This reflects a balance between the two- and three-body forces.

Table IV. The Average Percentage Changes of Total Energy between the Lennard-Jones and Many-Body Potentials Described in the Text as a Function of Nuclearity[a]

no. of atoms	% change (minima)	% change (transition states)
5	3.0	3.9
7	4.6	5.1
8	5.3	5.6
13	7.1	7.5
14	7.5	7.8
33	11.2	10.7
55	11.8	11.9

[a] The results are broken down into minima (left) and transition states (right).

Table V. The Average Three-Body Energy Expressed as a Percentage of the Two-Body Energy for the Many-Body Potential Described in the Text Analyzed as a Function of Nuclearity[a]

no. of atoms	$\overline{\lvert V_3/V_2 \rvert} \times 100$ (minima)	$\overline{\lvert V_3/V_2 \rvert} \times 100$ (transition states)
5	2.6	2.2
7	3.0	2.8
8	3.1	3.0
13	4.0	3.8
14	4.3	3.9
33	4.7	4.5
55	5.1	5.1

[a] The results are broken down into minima (left) and transition states (right).

We can also analyze the three-body contribution to the total energy as a percentage of the two-body energy according to nuclearity and the order of the stationary points (Table V). The results are in good agreement with those of Etters and Danilowicz[30] for the minima, rising from around 2.6% for Ar_5 to 5.1% for Ar_{55}. The percentage rises with increasing nuclearity because surface effects become progressively less important. The presence of the surface reduces the number of three-body terms more than the number of two-body terms, and so the bulk percentage contribution of around 10% is only approached for larger clusters. The average percentage is always somewhat smaller for transition states then minima, because the more open transition-state geometries affect the three-body terms more than the two-body terms.

V. Discussion

Having examined some balanced structures in detail and the effect of including three-body terms for a wide range of small and intermediate sized argon clusters, we now turn to some qualitative discussions of the relationships between cluster structures and potentials. To do this we must examine not only balanced structures, and the changes in the order of these stationary points in different systems, but also minima that are not balanced geometries. Carbon compounds provide a simple example. Stable species, such as cubane and dodecahedrane, are systems in which each carbon atom is essentially tetravalent, and therefore we expect these balanced structures to be minima. In contrast, the trigonal bipyramidal structures $C_5H_5^+$ and $C_5H_5^-$ are saddles of order five (see Table I). The structural relationships revealed for borohydrides, argon clusters, and "trapped ion" clusters are rather more interesting, especially as we would also like to extend this discussion to the more complex problem of the bonding in transition-metal clusters.

Deltahedra, where all the faces are triangular, are clearly the most important structures for borohydrides, "trapped ion" clusters, and argon clusters, as well as for many transition-metal clusters. In the case of argon and transition-metal clusters minima generally have centered geometries, but this is never the case for borohydrides or carboranes. For "trapped ion" clusters minima are sometimes possible with or without a central atom being present if the system is sufficiently large.[18] However, the unbalanced structures exhibited by these systems may be different. For example, the dodecadeltahedron is a minimum for $B_8H_8^{2-}$ and Ar_8 and a transition state for $(Be^+)_8^1$, whereas the square-antiprism

is a minimum for $(Be^+)_8^1$ and an order two saddle[8] for $B_8H_8^{2-}$. Furthermore, the D_{5h} bicapped pentagonal prism and the cuboctahedron are true transition states for icosahedral $(Be^+)_{12}^1$ and centered icosahedral $(Be^+)_{13}^1$, but not for $B_{12}H_{12}^{2-}$ and Ar_{13}.

Argon clusters are the easiest to understand. Here the most important factor is connectivity, and the maximization of coordination number leads to deltahedral minima for small clusters and centered deltahedral structures for larger species. The latter can also be described as polytetrahedral structures, which are commonly observed for transition-metal clusters too, as Johnson and Woolley have noted.[31] The principle of maximization of coordination number may also be responsible for the favorable Mackay icosahedral morphologies[32] of colloidal gold and silver particles, as discussed elsewhere.[33] By using appropriate transformations within a molecular orbital framework it is possible to show that the spectrum of molecular orbitals is wider for structures of higher connectivity.[33] Although this is only a qualitative argument, and other factors are also involved, connectivity is clearly of great importance for many covalent and van der Waals clusters. We will return to this point below.

First, however, it is important to note the difference between deltahedral covalent and van der Waals clusters and "trapped ion" clusters, namely that in "trapped ion" clusters the ions explicitly repel rather than attract one another. In "trapped ion" clusters there is therefore a driving force to maximize the inter-ion distances in the surface while minimizing the average radius of the shell of atoms. Although deltahedra maximize the number of nearest neighbor contacts they also provide the most effective coverage of a spherical surface and therefore minimize the shell radius for a given nearest-neighbor separation. Another important factor is that the bare Coulombic repulsion of the trapped ions is significantly longer ranged that the Lennard-Jones potential, and presumably the effective interatomic forces in covalent clusters. Hence, although deltahedra maximize the number of nearest neighbors they have relatively large second-nearest-neighbor distances. Overall, deltahedral geometries can therefore be the optimal solutions to both the attractive Lennard-Jones packing problem and the repulsive "trapped ion" cluster problem.

The non-deltahedral "trapped ion" clusters illustrate the delicate balance of forces for these systems, where square faces appear to be much more favorable than for argon clusters or borohydrides. In the latter molecules, which must be described by relatively shorter range attractive effective potentials, square faces will generally raise the energy. However, in "trapped ion" clusters the balance between the Coulombic repulsion (which favors square over triangular faces) and the average radius appears to be more delicate. This explains why diamond–square–diamond processes[3] are often so facile in these systems.[1,18]

Finally we should ask why centered polytetrahedral geometries are often favorable for argon[14] and transition-metal clusters,[34] whereas non-centered deltahedra are generally favored for borohydrides and hydrocarbon clusters.[34] The answer to this problem has already been discussed in terms of bonding theories for transition-metal and main-group clusters;[35] however, our object here is to try and understand the trends in terms of effective potential functions. Argon clusters probably provide the simplest examples, and the prevalence of icosahedral packing schemes has been interpreted in terms of the isotropic well pair potential.[33] It seems likely, then, that the deltahedral single-shell structures exhibited by borohydrides and carboranes can be rationalized in terms of a relatively isotropic effective potential in the surface of the sphere, but with a directional radial component.

To test this hypothesis potential surfaces were calculated for the angular displacement of a single CH or BH unit in prismane, C_6H_6, and $B_6H_6^{2-}$, respectively. The SCF energy was calculated over a grid of angular θ,ϕ displacements starting from the equilibrium optimized STO-3G geometries. For prismane the angular coordinates of the chosen CH unit were (θ,ϕ) = (48.31°,0°); the constant radii were 1.170 and 2.251 Å for carbon and hydrogen, respectively. For $B_6H_6^{2-}$ the corresponding parameters of the chosen vertex were (90°,0°) with r_B = 1.1894 Å and r_H = 2.3491 Å. These parameters uniquely define the equilibrium geometries. In both cases θ and ϕ were varied through ±20° except that symmetry equivalent geometries were not repeated. The axis systems and calculated surfaces are shown in Figure 4, where we see that the $B_6H_6^{2-}$ surface is indeed remarkably isotropic in terms of angular displacements. This is not the case for prismane, where the energy increases more rapidly when we stretch or compress the axial C–C bond by changing θ. The energy changes least rapidly for displacements of the ϕ coordinate with a corresponding small increase in θ (which helps to preserve the axial C–C bond). These results agree very well with theoretical descriptions of cluster bonding where delocalized systems such as $B_6H_6^{2-}$ are treated by separating the radial and tangential basis atomic orbitals.[35,36] Systems that can be understood in terms of localized two-electron bonds clearly have anisotropic potential surfaces for angular displacements of the vertices.

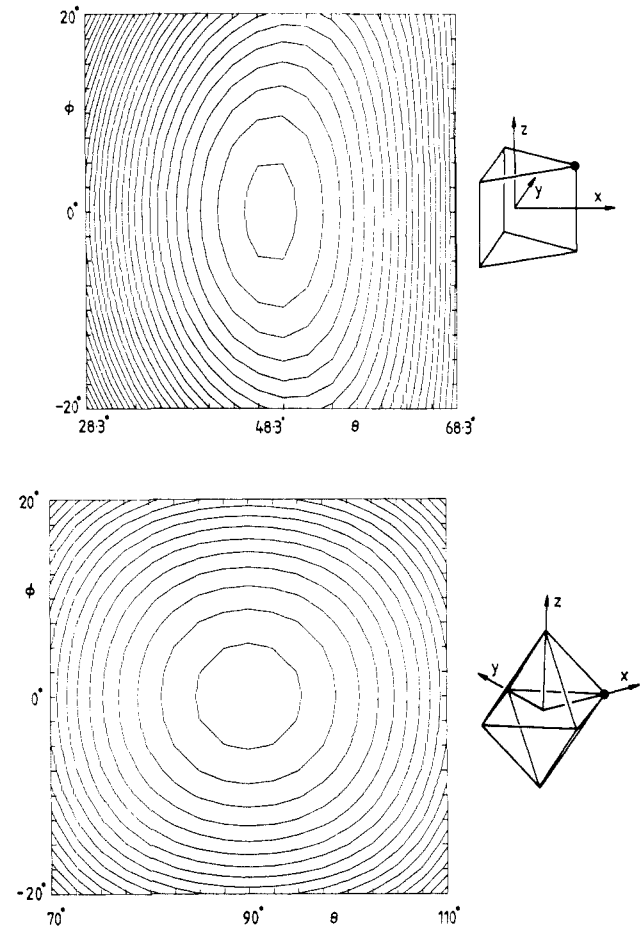

Figure 4. Potential energy surfaces for the angular displacement of the (θ,ϕ) = (48.31°,0°) CH unit in prismane (top) and the (90°,0°) BH unit in $B_6H_6^{2-}$ (bottom). The energy range for prismane is 7.6 eV with contours spaced at intervals of 0.27 eV, and the corresponding parameters for $B_6H_6^{2-}$ are 4.8 and 0.24 eV, respectively. The axis systems and skeletal vertices that are displaced are indicated schematically in each case. The grid spacings are 2.5° × 2.67° and 2.5° × 2.5°, respectively, giving 272 and 289 data points for the two plots.

The above discussions are intended to provide some qualitative explanations for the sort of trends observed in the various types

(31) Johnson, B. F. G.; Woolley, R. G. *J. Chem. Soc., Chem. Commun.* **1987**, 634.
(32) Mackay, A. C. *Acta Crystallogr.* **1962**, *15*, 916.
(33) Wales, D. J.; Kirkland, A. I.; Jefferson, D. A. *J. Chem. Phys.* **1989**, *91*, 603.
(34) See, for example: Cotton, F. A.; Wilkinson, G. *Advanced Inorganic Chemistry*, 5th ed.; John Wiley: New York, 1988.
(35) Wales, D. J. *Mol. Phys.* **1989**, *67*, 303.
(36) Stone, A. J. *Mol. Phys.* **1980**, *41*, 1339.

of cluster discussed in this paper. In particular, explanations framed in the language of effective potentials for covalent clusters, using analogies with other, simpler systems, provide an alternative way of looking at the structures of these molecules. More quantitative analyses may also be possible in future work. Balanced structures provide a particularly helpful set of examples because we know in advance that they must be stationary points of some order, and the variation of the order with the type of potential may be most illuminating. Furthermore, balanced structures suggest possible structures for new stable species; for example, it would be interesting to investigate icosidodecahedral $B_{30}H_{30}^{2-}$, or even C_{30}, to see if this structure is ever a minimum or a transition state.

Acknowledgment. The computer time for this work was funded in part by a Grant from the National Science Foundation to Prof. R. S. Berry, whose hospitality throughout the author's stay in Chicago under a Lindemann Trust Fellowship is greatly appreciated. Dr. J. F. Stanton provided helpful advice on the use of the ACES optimiser. I am also grateful to the referees for some constructive criticisms of the original manuscript and to Dr. A. J. Stone for several discussions.

Electron-Tunneling Pathways in Ruthenated Proteins

David N. Beratan,*[†,‡] José Nelson Onuchic,[†,‡,§] Jonathan N. Betts,[‡] Bruce E. Bowler,[‡,∥] and Harry B. Gray[‡]

Contribution from the Jet Propulsion Laboratory, California Institute of Technology, Pasadena, California 91109, Beckman Institute,[⊥] California Institute of Technology, Pasadena, California 91125, Instituto de Física e Química de São Carlos, Universidade de São Paulo, SP, Brazil, and Department of Physics, University of California, San Diego, La Jolla, California 92093. *Received December 8, 1989*

Abstract: We implement a numerical algorithm to survey proteins for electron-tunneling pathways. Insight is gained into the nature of the mediation process in long-distance electron-transfer reactions. The dominance of covalent and hydrogen bond pathways is shown. The method predicts the relative electronic couplings in ruthenated myoglobin and cytochrome *c* consistent with measured electron-transfer rates. It also allows the design of long-range electron-transfer systems. Qualitative differences between pathways arise from the protein secondary structure. Effects of this sort are not predicted from simpler models that neglect various details of the protein electronic structure.

I. Introduction

Long-distance electron transfer in proteins involves electron tunneling through a polypeptide environment.[1] Although donor–acceptor electronic interactions in many proteins are relatively weak, they are not as weak as would be expected in the absence of the polypeptide bridge.[2] Theory suggests that the transfer rate should be sensitive to the molecular details of the tunneling bridge in a weakly coupled donor–acceptor molecule and that a molecular orbital approach is an appropriate one.[3]

Methods to calculate weak bridge-mediated donor–acceptor interactions have been of interest for some time in chemistry.[1,2] We recently developed a model for the dependence of the donor–acceptor coupling and transfer rate on bridge structure in small molecules[2e,4] and proteins.[5] While refinements[5b] are being added to the protein model (questions still remain concerning details of the electronic structure techniques[5c] and the density of important pathways, see next section), the model provides a framework for the interpretation and design of experimental systems.

In this paper we present a numerical implementation of our theoretical model for electron tunneling in proteins. The model divides the bridge that assists the electron-tunneling process into a number of blocks. The decay of the interaction across each block is sufficiently rapid that the overall coupling can be approximated as a product of decays per block where these decays depend only on the details of the particular block and the tunneling energy.[5] This approximation is an oversimplification based in perturbation theory, and strategies to generalize this treatment are discussed in the following sections. The description of the bridge as a combination of identifiable blocks is a useful one that applies even beyond the perturbation theory limit.[6] This is a central theme of our model, and future implementations that take more details of the bridge into account will be based on this description.

These blocks of orbitals between donor and acceptor define pathways that mediate electron transfer. Due to the approximately *exponential* decay of the coupling with the number of bridging groups in a tunneling pathway, one expects relatively few pathways to be important for coupling the donor and acceptor in a given protein or protein–protein complex. If gating of the electron-transfer reaction[7] becomes important, the calculation of the tunneling matrix element for the relevant pathway must be

[†] Jet Propulsion Laboratory, California Institute of Technology.
[‡] Beckman Institute, California Institute of Technology.
[§] University of California, San Diego, and Instituto de Física e Quimica de São Carlos.
[∥] Present address: Department of Chemistry, University of Denver, Denver, CO 80208.
[⊥] Contribution No. 8086.

(1) (a) Marcus, R. A.; Sutin, N. *Biochim. Biophys. Acta* **1985**, *811*, 265. (b) Newton, M. D.; Sutin, N. *Annu. Rev. Phys. Chem.* **1984**, *35*, 437. (c) *Photoinduced Electron Transfer*; Fox, M. A., Chanon, M., Eds.; Elsevier: Amsterdam, 1988; Vols. A–D.
(2) (a) Halpern, J.; Orgel, L. E. *Discuss. Faraday Soc.* **1960**, *29*, 32. (b) McConnell, H. M. *J. Chem. Phys.* **1961**, *35*, 508. (c) Hopfield, J. J. *Proc. Natl. Acad. Sci. U.S.A.* **1974**, *71*, 3640. (d) Larsson, S. *J. Am. Chem. Soc.* **1981**, *103*, 4034. (e) Beratan, D. N.; Hopfield, J. J. *J. Am. Chem. Soc.* **1984**, *106*, 1584. (f) Riemers, J. R.; Hush, N. S. *Chem. Phys.* **1989**, *134*, 323.
(3) Beratan, D. N.; Onuchic, J. N.; Hopfield, J. J. *J. Chem. Phys.* **1985**, *83*, 5325.
(4) (a) Onuchic, J. N.; Beratan, D. N. *J. Am. Chem. Soc.* **1987**, *109*, 6771. (b) Beratan, D. N. *J. Am. Chem. Soc.* **1986**, *108*, 4321.
(5) (a) Beratan, D. N.; Onuchic, J. N.; Hopfield, J. J. *J. Chem. Phys.* **1987**, *86*, 4488. (b) Onuchic, J. N.; Beratan, D. N. *J. Chem. Phys.* **1990**, *92*, 722. (c) Beratan, D. N.; Onuchic, J. N. *Photosynth. Res.* **1989**, *22*, 173.
(6) da Gama, A. A. S. *J. Theor. Biol.* **1990**, *142*, 251.
(7) Hoffman, B. M.; Ratner, M. A. *J. Am. Chem. Soc.* **1987**, *109*, 6237.

0002-7863/90/1512-7915$02.50/0